Journal Name

ARTICLE

Efficient removal of metal ions by capacitive deionization with straw waste derived graphitic porous carbon nanosheets

Hui Wang[a,b,†], Tingting Yan[a,†], Junjie Shen[c], Jianping Zhang[a], Liyi Shi[a] and Dengsong Zhang[a]*

Received 00th January 20xx,
Accepted 00th January 20xx

DOI: 10.1039/x0xx00000x

www.rsc.org/

Capacitive deionization (CDI) is considered to be an energy-efficient and cost-effective technology for ions removal from saline or waste water. However, its implementation remains challenging due to low ion adsorption capacity of the commonly used electrode materials. It is thus desirable to develop highly efficient CDI electrode materials for ions removal. Herein, graphitic porous carbon nanosheets (GPCS) were originally prepared from the straw waste via a combined activation and graphitization process. Composed of graphitic carbon sheets with abundant pores in the framework, the obtained GPCS had large specific surface area, good conductivity and wettability, which can provide sufficient adsorption sites and promote efficient ion transport. The GPCS electrodes presented higher specific capacitance, good stability and low inner resistance in the electrochemical tests. Moreover, the GPCS showed a high deionization capacity of 19.3 mg g^{-1} at 1.2 V in a 500 mg L^{-1} NaCl solution. The repeated adsorption-desorption experiments demonstrated the good regeneration performance of GPCS electtrodes. Furthermore, the removal efficiency of Cd^{2+}, Ni^{2+} and Cu^{2+} by GPCS elelctrodes is 91.5%, 97.0% and 100% at 1.2 V in a 100 mg L^{-1} $CdCl_2$ solution , $NiCl_2$ or $CuCl_2$ solution. This work offers a promising solution to efficient removal of ions from saline or waste water and a new route to the utilization of straw waste.

Environmental significance

Fresh water scarcity has become one of most great critical problem due to the worsening water quality from pollution as well as the growing population. Capacitive deionization has been regarded as a promising water treatment technology to obtain fresh water. However, developing highly efficient electrode materials for capacitive deionization remains challenging. Here, a simple and low-cost method was developed to prepare graphene-like hierarchical porous carbon nanosheets (GPCS) from straw waste as highly efficient electrode materials for capacitive deionization. Significantly, the obtained GPCS was composed of graphitic carbon sheets with abundant pores in the frameworks. Importantly, the GPCS exhibited large specific surface area, good wettability and electronic conductivity. Moreover, the GPCS electrodes showed a high deionization capacity of 19.3 mg g^{-1} at 1.2 V in a 500 mg L^{-1} NaCl solution. The removal efficiencies towards Cd^{2+}, Ni^{2+} and Cu^{2+} were higher than 90%. Additionally, the electrodes presented good deionization stability. The current work offers a promising solution to efficient removal of ions from saline or waste water and a new route to the utilization of straw waste.

Introduction

Recently, the shortage of fresh water has become one of the most serious problems around the world due to water pollution and growing population.[1,2] Water desalination proves efficient to solve the water crisis, and conventional desalination techniques such as thermal processes and reverse osmosis were extensively employed to separate ions from water.[3, 4] However, significant cost and excessive energy consumption restricted the wide application of traditional techniques. Moreover, to obtain fresh water, the waste water treatment, especially the deep removal of excess metal ions from water is also important and challenging. Emerging as a promising water treatment technique, capacitive deionization (CDI) has drawn great attention, and has been used for heavy metal removal, organic pollutants removal, and desalination. [5-7] The CDI process is based on the mechanism of electrical double-layer capacitor. When operated with a low external voltage (< 2 V), ions are moved to the opposite charged electrode and adsorbed within the electrical double-layer (EDL) formed between the solution and the electrode interface. Once the voltage is removed, the ions adsorbed by the electrodes can be released to the solution immediately. Therefore, CDI provides an energy-saving and environmental-friendly method to obtain clean water. [8, 9]

As an electrochemical process, the CDI performances are largely determined by the internal structure and physical properties of the electrode materials, such as specific surface area, pore structure, conductivity and wettability.[10, 11] Till now, various carbon materials such as activated carbon, carbon

[a] Department of Chemistry, Research Center of Nano Science and Technology, State Key Laboratory of Advanced Special Steel, Shanghai University, Shanghai 200444, P. R. China. E-mail: dszhang@shu.edu.cn.
[b] School of Environmental Science and Engineering, Yancheng Institute of Technology, Yancheng, 224051, P. R. China.
[c] Department of Chemical Engineering, University of Bath, Bath BA2 7AY, UK
† H.W. and T.Y contributed equally to this work.

Electronic Supplementary Information (ESI) available: The SEM image of the GPCS, the SEM and TEM images of PC, CC and APC; XPS survey scan spectra and FTIR spectra of GPCS, PC, CC and APC; CV curves of the GPCS obtained from different calcination temperature at 10 mVs^{-1} in a 0.5 M NaCl solution; CV curves at 10 mV/s, GC curves at 0.2-1.0 A/g; current transient and plot for pH vs. time for GPCS electrodes in a 500 mg L-1 NaCl solution at 1.2 V; adsorption kinetics parameters of GPCS, PC, CC and APC.]. See DOI: 10.1039/x0xx00000x

nanotube, carbon aerogel, mesoporous carbon and graphene have been widely employed as CDI electrodes.[12-17] Especially, graphene with ultra-high theoretical surface area and conductivity has attracted great interest in the past decade. Li et al. reported that graphene-like nanoflakes showed higher electrosorption capacity than activated carbon.[18] However, owing to the π-π interactions and van der Waals force between the planer basal planes, graphene sheets can spontaneously undergo aggregation and restacking, which will largely decrease the accessible surface area for ion adsorption.[19, 20] Several methods such as intercalation of objective carbon materials, and design of three dimensional structure were recently investigated to overcome this problem.[21, 22] However, these new methods are complicated, and have high costs and low yields. As a result, graphene-based materials can hardly meet the scale-up requirements for commercial CDI.

In consideration of the above-mentioned problems, it is highly desirable to develop CDI electrode materials through a cost-effective and simple route with the potential for achieving mass production. Biomass, as a low-cost and abundant carbon source, can be easily obtained from forestry and agricultural wastes. [23-25] Recently, various biomasses have been explored as carbon source, and different strategies were applied to enhance the performance of biomass-derived carbons. For example, Ding et al. used peanut shells derived carbon as the active materials in both the anode and the cathode of a hybrid sodium ion capacitor.[23] Wu et al. demonstrated that honeycomb-like porous carbon foam produced from one-step carbonization of alkali-treated wheat flour showed excellent electrochemical performance for supercapacitor electrodes.[25] Xie et al. prepared carbon materials from citrus peel through hydrothermal synthesis with $ZnCl_2$.[26] Cazetta et al. found that the adsorption capacity of biomass-derived carbon catalyzed by iron was greatly increased.[27] Straw is a by-product of agricultural crops, which is abundant in the nature. A large number of wheat straws have been produced annually with the increasing wheat production. However, only small amounts of wheat straws are used as animal feed, and most of them are treated as wastes and cause some environmental problems. Thus, it is highly beneficial to use the straw waste as carbon sources and develop the simple and easy synthesis routes.

In this study, efficient CDI of saline or waste water was demonstrated by using the graphitic porous carbon nanosheets (GPCS). We provided a novel approach to design and synthesize GPCS derived from straw waste via a combined activation and graphitization process. The brief synthesis route of GPCS was illustrated in Scheme 1. The metal salts ferric chloride ($FeCl_3$) and zinc chloride ($ZnCl_2$) acted as the graphitization catalyst precursor and the activation agent, respectively. They were simultaneously introduced into straw framework. During the high temperature calcination process, the Zn species as activation agent introduced plentiful micro- and mesopores to the carbon nanosheets, and resulted in high specific surface area. Besides, as a graphitization catalyst, Fe compounds in the straw skeleton led to carburized phases, and graphitic nanosheets were formed after the decomposition of carburized phase in the calcination. The GPCS were obtained after the complete removal of Fe compound and other impurities. The GPCS showed remarkable features, such as hierarchical pores, large surface area and nanosheet structure, which could promote fast salty ion transfer and adsorption during the CDI process. Therefore, we successfully developed a cost-efficient and renewable raw carbon material for high performance CDI.

Experimental section

Chemicals

$FeCl_3$, $ZnCl_2$, $CdCl_2$, $NiCl_2$, $CuCl_2$ and hydrochloric acid (HCl) of analytic grade were purchased from Sinopharm Chemical Reagent Co. Ltd., Shanghai, China. The wheat straw was from Yancheng, Jiangsu, China. Before use, the wheat straw was washed by deionized water and ethanol for several times.

Synthesis

Pre-carbonization of the wheat straw: 1.5 g wheat straw and 2.5 mL H_2SO_4 were added into 50 mL H_2O and then stirred for 20 min. The above solution was transferred into the Teflon vessel and reacted for 12 h at 180 ^oC. After cooling to the room temperature, the pre-carbonized wheat straw was washed using deionized water until reaching a pH of 7, and further drying at 80 ^oC in a conventional oven, then the pre-carbonized wheat straw was obtained.

Synthesis of GPCS: 1.0 g pre-carbonized wheat straw and 2.5 g $ZnCl_2$ were immersed in the 20 mL of 2.5 M $FeCl_3$ solution. The mixed solution was continuously stirred and evaporated at 80 ^oC until it became viscous, and dried at 80 ^oC in a conventional oven. The obtained solid powder was further annealed at 700 ^oC for 1 h under a N_2 atmosphere at a ramp rate of 2 ^oC/min. To remove metal species and silica, the obtained black powder was etched with HCl solution (2 M) and HF solution (10 wt%), and then thoroughly washing with deionized water and drying at 80 ^oC, the GPCS were finally obtained. For comparison, pre-carbonized wheat straw annealed without $ZnCl_2$ and $FeCl_3$ was named as the porous carbon (PC). Pre-carbonized wheat straw annealed with $FeCl_3$ only was named as the catalyzed carbon (CC). Pre-carbonized wheat straw annealed with $ZnCl_2$ only was named as the activated porous carbon (APC).

Characterization

The structure and surface properties of obtained carbon materials were investigated by transmission electron microscopy (TEM), scan electron microscopy (SEM), X-Ray diffraction (XRD), Raman, N_2 sorption, wettability measurements. Besides, the related electrodes were further analysed by cyclic voltammetry (CV), Galvanostatic charge-discharge (GC) and electrochemical impedance spectroscope (EIS). The detail information of those characterization was provided in the supporting information (SI).

CDI performance

To fabricate the CDI electrodes, the as prepared carbon materials (80 wt%) and conductive carbon black (10 wt%) were homogenously mixed with the binder (PTFE, 10 wt%). The mass

Journal Name

ARTICLE

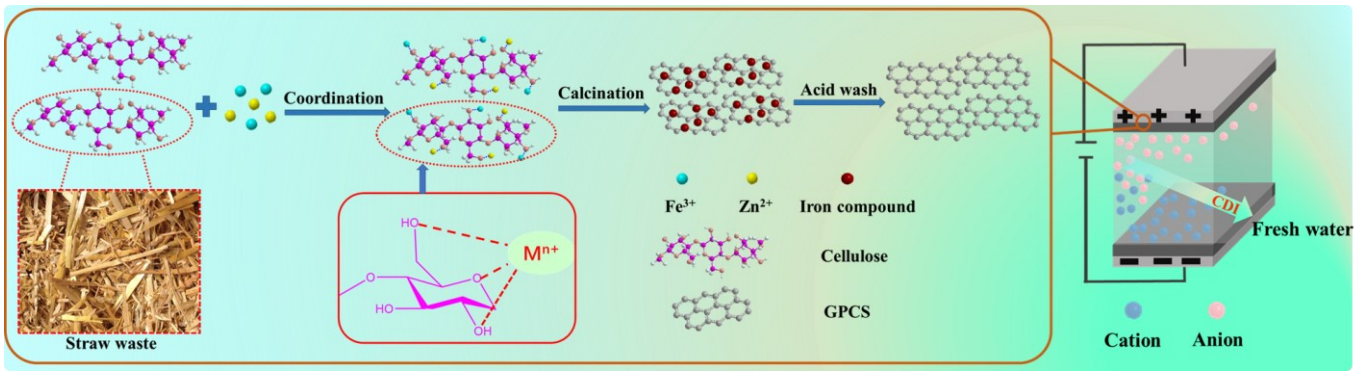

Scheme 1 Schematic illustration of the fabrication of GPCS for CDI.

of active materials is 0.2 g. The above slurry was coated onto graphite sheets and then the electrodes were dried at 110 °C overnight. The size of electrode is 50 mm × 40 mm × 0.3 mm. The CDI system consists of two electrodes separated by a non-conductive grid spacer (0.27 mm). The CDI experiment was performed at the set voltage with a flow rate of 50 mL min^{-1} using a peristaltic pump. The NaCl solution conductivity change was monitored by a conductivity meter (Mettler Toledo S400) at the outlet of the cell. The concentration of Cd^{2+}, Ni^{2+} and Cu^{2+} was detected by atomic absorption spectrometer (Persee, TAS900). The salt adsorption capacity (SAC) and salt (SAR) were calculated as below:

$$\mathbf{SAC} = \frac{(\mathbf{C_0} - \mathbf{C}) \times \mathrm{V}}{\boldsymbol{m}} \qquad (1)$$

$$\mathbf{SAR} = \frac{\mathbf{SAC}}{\boldsymbol{t}} \qquad (2)$$

Where C_0 is initial concentration (mg L^{-1}), and C is concentration at any time (mg L^{-1}), V is the solution volume (L), m is the electrode mass (g) and t is the deionization duration (min).

Results and discussion

Characterization of structure and micromorphology

The pore structure characteristics of GPCS, APC, CC and PC were detected by the nitrogen adsorption-desorption isotherm. As shown in Fig.1a, all the carbon samples exhibit a type-I adsorption-desorption isotherms, indicating a microporous structure.[28-30] Moreover, the adsorption isotherms of samples at the low relative pressure increased sharply, which further indicates that micropores dominate the carbon structure. In the inset, a hysteresis loop ($0.4 < P/P_0 < 1.0$) is appeared on the isotherm of GPCS, suggesting the coexistence of micropore and mesopore. More interestingly, the isotherms of GPCS, APC and

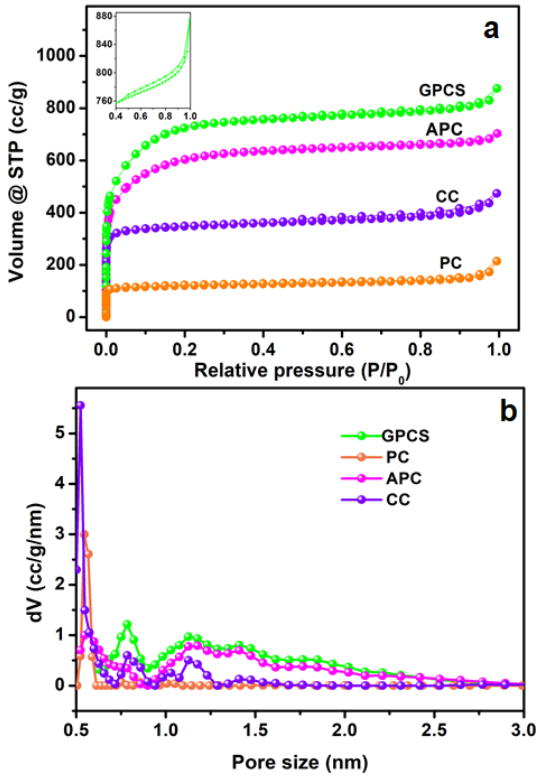

Fig.1 N_2 adsorption-desorption isotherms and pore size distribution of the GPCS, APC, CC and PC. The Inset of (a) is the isotherm at $0.4 < P/P_0 < 1.0$.

CC show wider knees than that of PC, suggesting their larger micropore sizes. As calculated, GPCS have the highest specific surface area of 2695 m^2/g and total pore volume of 1.15 cm^3/g. APC with only Zn activation has the second highest specific surface (2207 m^2/g) and the second largest pore volume (0.95 cm^3/g). CC carbonized only with Fe catalyst exhibits a lower specific surface area of 1371 m^2/g and a smaller pore volume of 0.63 cm^3/g. PC has the lowest specific surface area of 493 m^2/g

Journal Name

ARTICLE

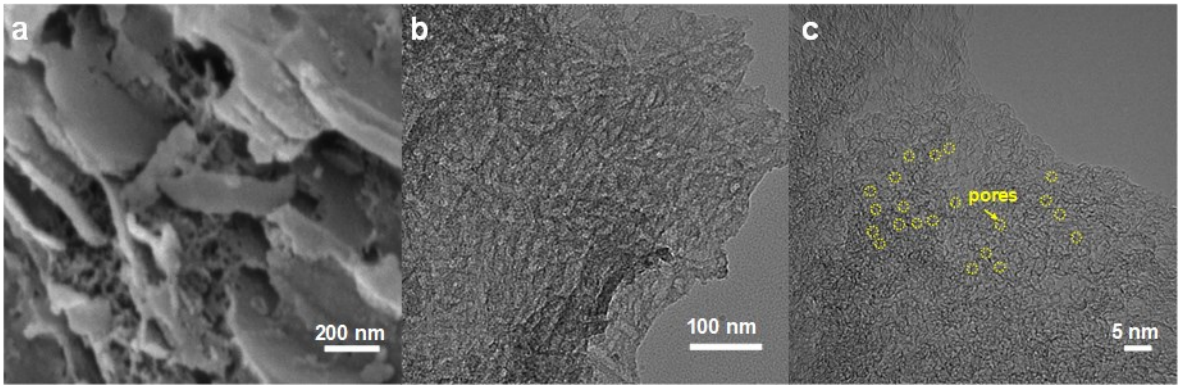

Fig.2 (a) SEM, (b) TEM and (c)HRTEM images of GPCS.

and the smallest pore volume of 0.24 cm^3/g. These results indicate that the activation agent $ZnCl_2$ is essential to increase the specific surface area of GPCS.[31] The pore size distributions deduced by QSDFT are presented in Fig.1b. Obviously, the GPCS has an enlarged pore size of 0.8 nm and 1.2 nm compared to PC (0.5 nm), which benefits from the synergistic reaction of activation and catalysis. The excellent pore structure of GPCS can provide abundant ion adsorption sites and shorten the ion diffusion path during the CDI process.

As seen from SEM and TEM images in Fig.2a-b, the GPCS present a sheet-like and porous structure. The HRTEM image (Fig.2c) shows that the GPCS may compose of several porous carbon sheets, and large amount micropores are distributed on the surface of carbon sheets. In particular, the edge of GPCS have no obvious lattice line in the HRTEM image, indicating that the GPCS also contain some structure defects and lattice disorder, which is beneficial to the rapid electron and ion transport during the CDI process.[32] In comparison, the SEM and TEM images of PC, APC and CC (Fig.S1) show a bulk structure without any pores and the sheets are much thicker, suggesting that the synergistic effect of iron catalysis and zinc activation is necessary for the formation of nanosheet structure.[33] During the high temperature calcination process, the iron components act as the graphitization catalyst to accelerate the formation of carburized phase, and the carburized phase reacts with the Zn components. The graphitic porous nanosheet structure of GPCS is finally formed with the synergistic reaction of activation and catalytic carbonization process.

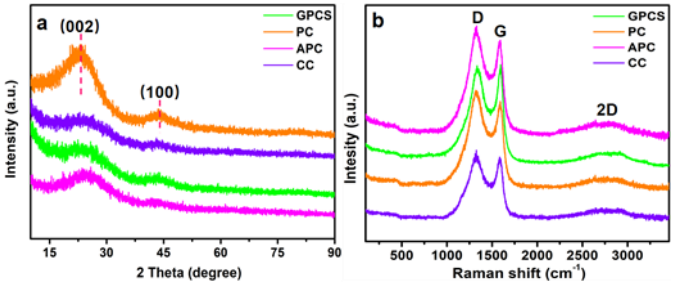

Fig.3 (a) XRD patterns and (b) Raman spectra of the GPCS, PC, APC and CC.

Fig.3a shows the XRD patterns of GPCS, APC, CC and PC. These samples have two broad diffraction peaks at $2\theta = 24^o$ and 43^o, which are similar to the graphitic carbon. The broad and weak peaks at 24^o and 43^o correspond to the (002) and (100) reflection of the graphitic-type lattice, which indicate a limited graphitization degree.[28] The (002) and (100) diffraction peaks of GPCS are weaker than those of PC and APC, because the individual graphene layers in the GPCS structure are disorderly arranged. The graphitization degree of the samples was further detected by Raman spectroscopy. D band (1370 cm^{-1}) corresponding to the disorder structures of carbon and G band (1570 cm^{-1}) relating to graphite in-plane vibrations are observed in Fig.3b.[24, 33] The I_G/I_D ratio of GPCS (1.01) is higher than those of PC (0.85), APC (0.88), and CC (0.93), indicating that the higher graphitization degree is due to the Fe catalysis. Besides, the GPCS show distinct 2D band at 2700 cm^{-1}. The higher graphitization degree of GPCS means the better electric conductivity, which is beneficial to lowering the inner resistance of GPCS electrode.

The dynamic contact angle measurements were further conducted for the GPCS, APC, CC and PC. The wetting processes are illustrated in Fig.4. At first, the contact angle of GPCS is 36.3^o, suggesting that the GPCS exhibit good hydrophily. Meanwhile the PC, APC and CC show much larger contact angles (129.0^o, 79.8^o and 111.7^o), which means poor wettability. After 0.5 s, the droplet on the surface of GPCS disappears and the contact angle reduced to 15.1^o. The droplet and contact angle of PC, APC and CC barely change within the same time. The results prove that droplet can be more easily adsorbed by GPCS, indicating that the GPCS have an improved wettability over other samples.[34] According to the XPS and FTIR analysis, the

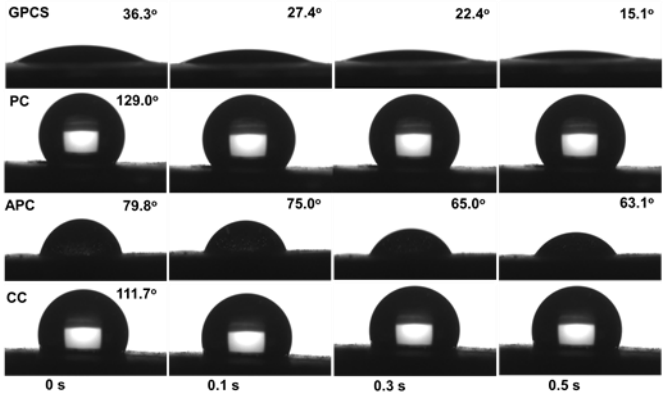

Fig.4 Optical micrographs of water contact angles on the surface of GPCS, PC, APC and CC electrodes as a function of contact time.

four samples have similar functional groups, but GPCS have the lowest oxygen and nitrogen contents (Fig.S2-3). Hence, the improved wettability of GPCS should be attributed to the abundant pores and sheet-like structure. With better wettability, GPCS can increase the accessible channels for metal ions, which is beneficial to the CDI performance.[35]

Electrochemical performance

The electrochemical performances of GPCS, APC, CC and PC in the NaCl solution were analysed to evaluate the CDI performance. As shown in Fig.5a, the CV curves of GPCS, APC, CC and PC demonstrate rectangular-like shape, and no redox peak was observed, which is indicative of typical EDLC behavior rather than pseudocapacitive behavior.[7, 36] Importantly, the GPCS electrode exhibits a much higher specific capacitance than that of PC, CC and APC, because the specific capacitance is linearly related to the CV curve area. As calculated, the GPCS electrode exhibits the highest specific capacitance of is 221.9 F g^{-1} at 1 mV s^{-1}, as compared to the APC, CC and PC electrodes (185.3, 171.7, 131.2 F g^{-1}). As the scan rate was increased to 10 mV s^{-1}, the CV curves were distorted due to less time for ion transportation and incomplete formation of EDL at higher scan rates. However, the CV curve area of GPCS electrode is still larger than those of PC, APC and CC at 10 mV s^{-1} (Fig.S4), indicating that a higher specific capacitance is well kept. Besides, the GPCS obtained from calcination at 700°C shows highest capacitance as compared to other temperature (Fig.S5). The 2D sheet-like structure of GPCS provide short ion diffusion distance, resulting in fast ion transportation.[37] Additionally, the highest specific surface area and pore volume of GPCS increase ion adsorption space and facilitate ion diffusion, and so more ions can participant in the formation of EDL. Besides, the GPCS with porous structure has good wettability, which allows salty solution to easily access the electrode interior. Therefore, GPCS exhibit higher specific capacitance in the CV tests, indicating that it is a promising material for CDI electrode.

The influence of ion concentration on the electrochemical performance of GPCS was investigated by the CV test, and the curves are presented in Fig.5b. When the salty solution concentration increases from 0.1 to 0.5 M, the area of CV curves increases accordingly, so the specific capacitance is improved with the increasing concentration. When ions are electrostatically adsorbed at the electrode/solution interface in a high concentration solution, the ionic strength of the solution changes slightly, and a new adsorption equilibrium can be quickly established. In contrast, the weak ionic-strength of low concentration solution results in a longer time for the new adsorption equilibrium formation.[38] Moreover, more ions can participate in the EDL forming process in higher concentration solution, so higher specific capacitance is easily obtained.[15]

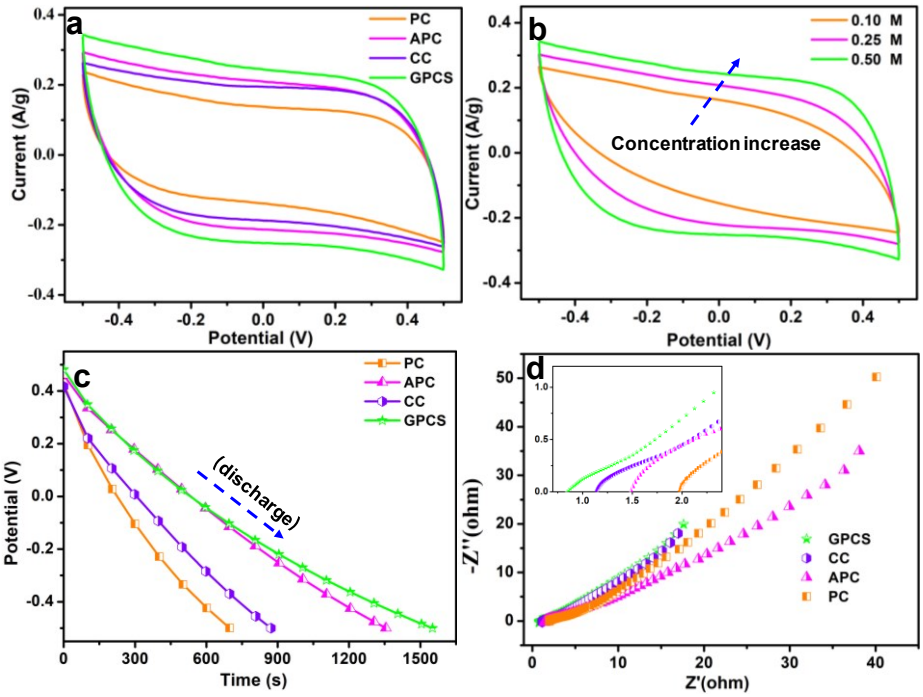

Fig.5 Electrochemical properties of the PC, APC, CC and GPCS electrodes. (a) cyclic voltammograms at a scan rate of 1 mV s^{-1} in a 0.5 M NaCl solution, (b) CV curves of GPCS electrodes at a scan rate of 1 mV s^{-1} in a NaCl solution with different concentrations, (c-d) GC curves at a current density of 0.2 A g^{-1} and the Nyquist plots in a 0.5 M NaCl solution. The inset of (d) is the expanded view in high-frequency region.

Journal Name

ARTICLE

The galvanostatic charge/discharge experiments of GPCS, APC, CC and PC electrodes were conducted at 0.2 A/g, and the discharge curves are shown in Fig.5c. Obviously, the GPCS electrode shows the longest discharge time as compared to PC, CC and APC, indicating highest specific capacitance. The enhanced capacitance further demonstrated that sheet-like structure, higher specific surface area and larger pore volume of GPCS is beneficial to capacitance increase. Besides, the GC curves are highly linear and symmetrical, indicating the ideal EDL behavior and rapid I-V response.[39] The charge-discharge curves remain symmetrical triangular shapes at different current densities ranging from 0.2 to 1.0 A g^{-1}, suggesting that the GPCS electrode can be smoothly charged and discharged at the given current densities (Fig.S6).

The EIS was commonly used to analyse the electrical resistance of electrodes during the electrochemical process. As shown in Fig.5d, the Nyquist plots contains a semicircle and straight line in the intermediate and low frequency region.[40] The semicircle represents the charge transfer resistance caused by Faradaic reactions at the interface is ignorable, indicating that all the electrodes have ultra-small charge transfer resistance. In the low frequency region, the straight line often relates to the capacitive behavior of the electrode. The straight lines of all the electrodes are deviated from the typical vertical line due to the slowed frequency dispersion and surface roughness of the electrodes.[41] The x-intercept in the high frequency region is related to the equivalent series resistance (ESR), associating to the intrinsic electronic properties of the electrode and salt solution, mass transmit resistance of the salt ion, and contact resistance between the current collector and the electrode.[42, 43] The ESR value of GPCS (0.88) is lower than those of CC (1.14), APC (1.48) and PC (1.96), indicating its reduced resistance. The following reasons have led to the above phenomenon: (i) The GPCS has an improved graphitization degree due to effective catalysis, and the electrical conductivity have been significantly improved; (ii) with 2D porous structure, the salty ions can easily diffuse in the GPCS structure. In contrast, the PC, APC and CC show a bulk structure with fewer ion transport channels, resulting in difficult mass transports. Therefore, the porous structure and higher graphitization degree together contribute to the much lower inner resistance of GPCS electrode. The EIS results further confirmed that GPCS with a reduced inner resistance and smooth electron/ion transport pathways is a good candidate for the CDI electrode material.

CDI performance

To investigate the CDI performance of GPCS electrodes, the batch mode flow-through deionization capacitor (FTDC) experiments were conducted in a NaCl solution with an initial conductivity of 1042 μS cm^{-1} at 1.2 V. The APC, CC and PC electrodes were also used for comparison. The plots of solution conductivity versus time are presented in Fig.6a. Once an external voltage was applied on the electrodes, the SAC rapidly increased. After about 30 min, SAC grows slowly until it reached the equilibrium. In the initial stage of CDI, electrode materials have enough adsorption sites for ion accumulation and adsorption. Besides, the electrostatic attraction between the adsorbed ion and electrodes is very strong at the electrode/solution interface. However, in a prolonged adsorption time, the number of adsorption sites is decreased and the electrostatic repulsion is enhanced, so the growth trend of SAC is slowed down. Particularly, the SAC of the GPCS electrode increases much more quickly as compared to the APC, CC and PC electrode, revealing that the GPCS electrodes exhibit higher adsorption rate and larger adsorption capacity. The SAC of GPCS reaches 19.3 mg g^{-1} after 40 min, much higher than those of PC, CC and APC (9.3, 13.3 and 14.3 mg g^{-1}) under 1.2 V in a 500 mg L^{-1} NaCl solution. In fact, the GPCS electrodes show obvious superiority as compared to recent publications (Table 1). It has been found in recent studies that a comprehensive consideration of SAC and SAR during the CDI process is necessary. [44, 45] When SAR is plotted against SAC, the Ragone comprehensive plots for CDI electrodes can be well obtained. In the Ragone plots of SAR versus SAC, the CDI performance of the electrodes can be visually presented. Fig.6b shows the comparison of the GPCS and PC electrodes in terms of the CDI performance. Apparently, the SAC increased with time until the adsorption equilibrium, while the SAR decreased with time. The slow growth of SAC and the rapid reduction of SAR during the CDI process can be attributed to the continuously reduced adsorption sites and enhanced electrostatic repulsion. More importantly, the Ragone plot of GPCS electrodes is located in the upper right region as compared to other electrodes, which reveals that the GPCS electrodes exhibit highest SAC and SAR. In addition, the adsorption behavior of GPCS in 500 mg L^{-1} NaCl solution can well described by the pseudo-second-order model with high correlation coefficient (0.9994). By contrast, the GPCS

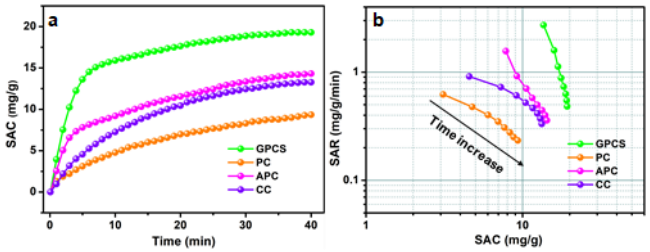

Fig.6 (a) Plots of SAC *vs* deionization time; (b) Ragone plots of SAR vs SAC for the GPCS, PC, APC and CC electrodes in a NaCl solution with a concentration of 500 mg L^{-1}.

Journal Name

ARTICLE

Table 1 Comparison of the CDI performance of various electrode materials in NaCl solution.

Electrode materials	Applied voltage(V)	Initial Concentration (mg L^{-1})	SAC (mg g^{-1})	Ref.
Hollow ZIFs-derived nanoporous carbon	1.2	500	15.31	[47]
Nitrogen-doped porous carbon nanofiber	1.2	1000	17.29	[48]
Phosphorus-doped 3D carbon nanofiber	1.2	1000	16.20	[49]
Hierarchical hole-enhanced 3Dgraphene	1.2	572	9.60	[50]
Protic salt-derived porous carbon	1.6	100	16.50	[51]
Ordered mesoporous carbon	1.2	500	10.80	[52]
Carbon beads	1.2	292	11.50	[53]
Nitrogen enriched activated carbon	1.2	1000	16.56	[54]
Porous graphene	1.2	500	6.26	[55]
Metal-organic framework/polypyrrole	1.2	584	11.34	[56]
Nitrogen-doped cluster-like	1.2	500	17.20	[35]
GPCS	1.2	500	19.30	This work

electrode shows the highest rate constant, demonstrating its good kinetic performance (Table S1). Besides, GPCS electrodes show a charge efficiency of 0.69, larger than those of PC (0.14), CC (0.45) and APC (0.32), which means GPCS electrodes have lowest energy consumption (Fig.S7). However, the charge efficiency of GPCS electrodes is less than 1.0, which is the result of the co-ion repulsion effect, binder blocking effect and the weak adhesion between electrodes and current collector.[46] The value of pH during the CDI process decreased slightly from 6.464 to 6.337, because a small amount of H^+ was released due to the oxidation of the anode (Fig.S8). The CDI performance of GPCS can be significantly improved after activation and catalysis, and the following reasons attributes to the enhanced performance of GPCS: (i) the larger specific surface area and pore volume of GPCS guaranteed enough active sites for ions accumulation; (ii) the nanosheet structure of GPCS reduces ion diffusion resistance and distance, and thus boosts the ion transportation; (iii) a large number of micropores on the GPCS structure promotes ion adsorption, which can ensure the full formation of the EDL. Besides, the pores on the surface of GPCS can connect independent carbon nanosheets and shorten the diffusion paths between carbon nanosheets, which can further promote ion migration; (iv) the GPCS show excellent wettability, so ions in the solution can easily immersed in the electrode. The inner pores of the electrode can be effectively utilized, and the accessible surface area of GPCS is further improved, which also favors the CDI performance; (v) the graphitization degree due to the effective iron catalysis, resulting in better electric conductivity. The GPCS with good conductivity can reduce the inner resistance, so the additional voltage consumption is decreased and more voltage can be used to adsorb salty ions during the CDI process. In conclusion, combining with high specific surface area, rich pore structure, high conductivity and wettability, the GPCS electrode is potential alternative for the CDI application.

The effect of salt concentration was further investigated to evaluate the CDI performance of GPCS. The initial concentration salty solution ranges from 100 to 500 mg L^{-1}, and the deionization results are presented in Fig.7a-b. As seen from the

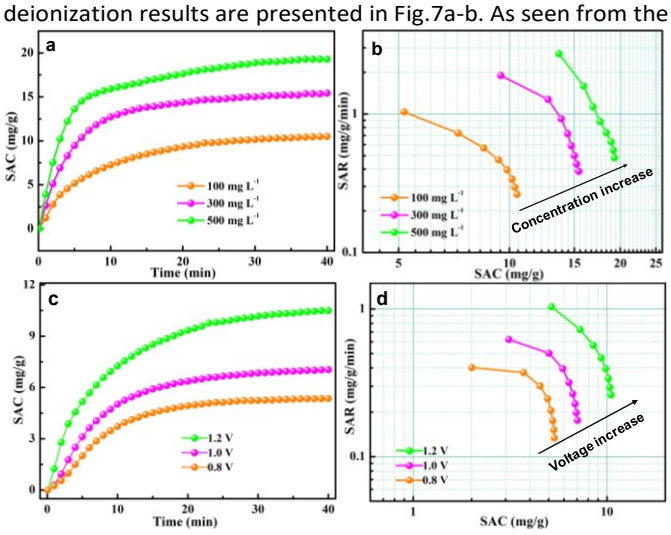

Fig.7 (a) plots of SAC *vs* deionization time; (b) Ragone plots of the GPCS electrodes under different concentration; (c) plots of SAC *vs* deionization time and (d) Ragone plots of the GPCS electrodes under different voltage. All the tests were conducted at the flow rate of 50 mL min^{-1}.

Fig.7a, the SAC is increased with the time until adsorption equilibrium and the growth trend of SAC is more obvious at higher concentration. As calculated, the SAC is 10.5, 15.4 and 19.3 mg g^{-1} in 100, 300 and 500 mg L^{-1} NaCl concentration. In Fig.7b, the Ragone plot shifted to the upper right region in higher concentration, indicating higher salt concentration can improve deionization capacity and rate. At higher salt concentration, the ionic conductivity is stronger, which is beneficial to rapid ion transfer into the electrodes. Besides, the higher NaCl concentration promotes a compact EDL formation, which accelerates the SAC increase.

The external voltage has a critical effect on the CDI efficiency.

It has been demonstrated that excessive voltage can cause Faraday reactions, and the aqueous solutions will be decomposed.[57-58] However, the low voltage will result in the incomplete EDL formation, and the adsorption capacity of electrode will be weakened accordingly.[57-58] Herein, the CDI performance of GPCS electrodes at 0.8-1.2 V in a 100 mg L^{-1} NaCl solution was carefully evaluated, and the results were shown in Fig.7c. The SAC increased with the deionization time, and the growth trend is particularly evident at a higher voltage. The GPCS electrodes can adsorb more salty ions at a higher voltage owing to the stronger coulombic interactions between electrodes and the oppositely charged ions. The SAC of the GPCS electrodes increased from 5.4 to 10.5 mg g^{-1}, when the voltage increased from 0.8 to 1.2 V. As shown in Fig.7d, the Ragone plot of GPCS electrodes is located in the upper right region at a higher voltage, suggesting the improved deionization capacity and rate due to the stronger coulombic interactions between ions and opposite charged electrode and a thicker EDL.

The regeneration performance is another important parameter to the CDI electrodes. Several multiple adsorption-desorption cycles of the GPCS electrode were further tested in a 100 mg L^{-1} NaCl solution, and both the adsorption and desorption processes last for about 10 minutes. The electrodes were applied with voltage in the adsorption process and then short-circuited in the desorption process. As shown in Fig.8a, the SAC has little change in the first five cycles, indicating that the electrode has good stability. Subsequently, the SAC decreased slightly, which may be caused by oxidation of the electrode surface during the prolonged cycles. This problem may be addressed by designing an asymmetric electrode using pseudocapacitive materials as the anode material in the future work. [59-60]

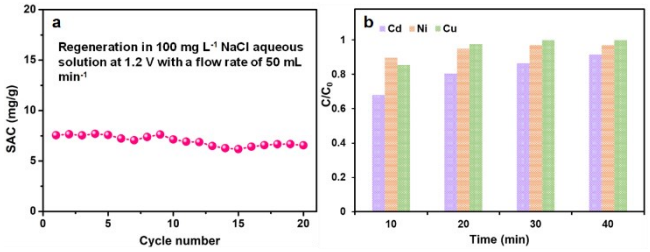

Fig.8 (a) Regeneration curves of the GPCS electrodes; (b) the adsorption efficiency of GPCS electrodes towards different metal ions in a 100 mg L^{-1} solution only containing Cd^{2+}, Ni^{2+} or Cu^{2+} at 1.2 V.

Excess metal ions in water environment pose a severe threat to human beings, and CDI technology provides an important method for the removal of excess metal ions. The removal performance of GPCS electrodes towards other typical metal ions are further studied. Fig.8b shows the adsorption efficiency of GPCS electrodes towards Cd^{2+}, Ni^{2+} and Cu^{2+} at 1.2 V in a 100 mg L^{-1} $CdCl_2$ solution, $NiCl_2$ or $CuCl_2$ solution. The removal efficiency of the GPCS electrodes increase with the adsorption time, and the removal efficiency of three metal ions by GPCS is higher than 90% at 40 min, indicating the metal ions can be effectively separated from water. As calculated, the adsorption capacities of GPCS electrodes towards Cd^{2+}, Ni^{2+} and Cu^{2+} are 13.7, 14.6 and 15.0 mg g^{-1} in a 100 mg L^{-1} $CdCl_2$ solution , $NiCl_2$ or $CuCl_2$ solution, higher than that of Na^+ (10.5 mg/g in a 100 mg L^{-1} NaCl solution) owing to the stronger electrostatic attraction between the CPCS electrode and the divalent metal ion. In summary, the porous structure, good wettability and conductivity make the GPCS electrode have adsorption properties for various metal ions.

Conclusions

In conclusion, efficient CDI of saline water has been demonstrated by using graphitic porous carbon nanosheets derived from straw waste. A sustainable route to convert biomass straw waste as a natural carbon source to graphitic porous carbon sheets was demonstrated. The fabrication process involved a facile method combining activation and catalysis to realize the 2D graphitic and porous structure. The obtained GPCS exhibited desirable characteristics including porous structure, good electrical conductivity and excellent wettability. In the electrochemical tests, the GPCS showed highest specific capacitance and lowest resistance as compared to the APC, CC and PC electrodes. In the CDI experiments, the unique structure and high surface area endowed GPCS with a high SAC (19.3 mg g^{-1}) and a high SAR (0.48 mg g^{-1} min^{-1}) in a 500 mg L^{-1} NaCl solution at 1.2 V. Moreover, the GPCS electrodes showed good regenerability in the repeated adsorption-desorption experiments. Furthermore, the removal efficiency of GPCS was higher than 90% towards different metal ions in 100 mg L^{-1} solution at 1.2 V. The work is valuable for designing carbon electrode materials by a sustainable and low-cost method and the utilization of straw waste.

Conflicts of interest

There are no conflicts to declare.

Acknowledgements

The authors acknowledge the support of the Natural Science Foundation of Jiangsu Province (BK20170475), National Natural Science Foundation of China (21906101), the Science and Technology Commission of Shanghai Municipality (19DZ2293100; 18DZ2281400; 17230741400), and the Royal

Academy of Engineering under the Research Fellowship scheme.

References

1 A. Subramani, J.G. Jacangelo, Water Res., 2015,**75**,164-187.
2 M.A. Shannon, P.W. Bohn, M. Elimelech, J.G. Georgiadis, B.J. Mariñas, A.M. Mayes, Nature, 2008, **452**, 301-310.
3 A. Macías-García, M. Gómez Corzo, M. Alfaro Domínguez, M. Alexandre Franco, J. Martínez Naharro, J. Hazard. Mater*., 2017,* **328**, 46–55.
4 M. Elimelech, W.A. Phillip, Science, 2011, **333**, 712-717.
5 J. Choi, P. Dorji, H.K, Shon, S. Hong, Desalination, 2019, **449**, 118-130.
6 S. Lopez-Bernabeu, R. Ruiz-Rosas, C. Quijada, F. Montilla, E. Morallon, Chemosphere, 2016, **144**, 982-988.
7 J. Kim, Y. Yi, D. H. Peck, S. H. Yoon, D. H. Jung and H. S. Park, Environ. Sci. Nano, 2019, **6**, 916-924.
8 C. Fan, S. Tseng, Z. Wu, K. Li, C. Hou, J. Hazard. Mater, 2016, **312**, 208-215.
9 L. Wang, J.E. Dykstra, S. Lin, Environ. Sci. Technol., 2019, **53**, 3366-3378.
10 H. Yin, S. Zhao, J. Wan, H. Tang, L. Chang, L. He, H. Zhao, Y. Gao, Z. Tang, Adv. Mater., 2013, **25**, 6270-6276.
11 S. Porada, R. Zhao, A. van der Wal, V. Presser, P.M. Biesheuvel, Pro. Mater. Sci., 2013, **58**, 1388-1442.
12 G. Wang, C. Pan, L.P. Wang, Q.G. Dong, C. Yu, Z.B. Zhao, J.S. Qiu, Electrochim. Acta, 2012, **69**, 65-70.
13 C. Y. Ma, S. C. Huang, P. H. Chou, W. Den, C. H. Hou, Chemosphere, 2016, **146**, 113-120.
14 J. Li, X. Wang, H. Wang, S. Wang, T. Hayat, A. Alsaedi, X. Wang, Environ. Sci. Nano, 2017, **4**, 1114-1123.
15 L.D. Zou, L.X. Li, H.H. Song, G. Morris, Water Res. 2008, **42**, 2340-2348.
16 R. Ruoff, Graphene: Calling all chemists, Nat. Nanotechnol. 2008, **3**, 10-11.
17 Z. P. Chen, W.C. Ren, L. B. Gao, B. L. Liu, S. F. Pei, H. M. Cheng, Nat. Mater., 2011, **10**, 424-428.
18 H. Li, L. Zou, L. Pan, Z. Sun, Environ. Sci. Technol. 2010, **44**, 8692-8697.
19 H. Wang, D. S. Zhang, T. T. Yan, X. R. Wen, J. P. Zhang, L. Y. Shi, Q. D. Zhong, J. Mater. Chem. A, 2013, **1**, 11778-11789.
20 Z. Y. Yang, L. J. Jin, G.Q. Lu, Q.Q. Xiao, Y. X. Zhang, L. Jing, X. X. Zhang, Y.M. Yan, K.N. Sun, Adv. Funct. Mater., 2014, **24**, 3917-3925.
21 X. Xu, Y. Liu, M. Wang, C. Zhu, T. Lu, R. Zhao, L. Pan, Electrochim. Acta, 2016, **193**, 88-95.
22 Z. U. Khan, T. T. Yan, L. Y. Shi, D. S. Zhang, Environ. Sci.: Nano, 2018, **5**, 980-991.
23 J. Ding, H.L. Wang, Z. Li, K. Cui, D. Karpuzov, X.H. Tan, A. Kohandehghanab and D. Mitlin, Energy Environ. Sci., 2015, **8**, 941-955.
24 C. Zhao, G. Liu, N. Sun, X. Zhang, G. Wang, Y. Zhang, H. Zhang, H. Zhao, Chem. Eng. J, 2018, **334**,1270-1280.
25 X. Wu, L. Jiang, C. Long, Z. Fan, Nano Energy, 2015, **13**, 527-536.
26 Z. Xie, X. Shang, J. Yan, T. Hussain, P. Nie, J. Liu, Electrochim. Acta, 2018, **290**, 666-675.
27 A. L. Cazetta, O. Pezoti, K.C. Bedin, T. L. Silva, A. Paesano Junior, T. Asefa, V.C. Almeida, ACS Sustain. Chem. Eng. 2016, **4**, 1058-1068.
28 S. S. Zhao, T. T. Yan, H. Wang, J. P. Zhang, L. Y. Shi, D. S. Zhang, ACS Appl. Mater. Interf., 2016, **8**, 18027-18035.
29 S. K. Park, H. Lee, M. S. Choi, D. H. Suh, P. Nakhanivej and H. S. Park, Energy Storage Mater., 2018, **12**, 331-340.
30 Z. L. Yu, S. Xin, Y. You, L. Yu, Y. Lin, D. W. Xu, C. Qiao, Z. H. Huang, N. Yang, S.H. Yu, J.B. Goodenough, J. Am. Chem. Soc., 2016, **138**, 14915-14922.
31 S. Uçar, M. Erdem, T. Tay, S. Karagöz, Appl. Surf. Sci., 2009, **255**, 8890-8896.
32 L. Sun, C. Tian, M. Li, X. Meng, L. Wang, R. Wang, J. Yin, H. Fu, J. Mater. Chem. A, 2013, **1**, 6462-6470.
33 H. Lei, T.T. Yan, H. Wang, L.Y. Shi, J.P. Zhang, D.S. Zhang, J. Mater. Chem. A, 2015, **3**, 5934-5941.
34 J. Zhang, J.H. Fang, J.L. Han, T.T. Yan, L.Y. Shi, D.S. Zhang, J. Mater. Chem. A, 2018, **6**, 15245-15252.
35 Y. Li, Y. Liu, J. Shen, J. Qi, J. Li, X. Sun, J. Shen, W. Han, L. Wang, Desalination, 2018, **430**, 45-55.
36 C. Chen, H. Wang, C. Han, J. Deng, J. Wang, M. Li, M. Tang, H. Jin and Y. Wang, J. Am. Chem. Soc., 2017, **139**, 2657-2663.
37 H. Wang, L. Zhi, K. Liu, L. Dang, Z. Liu, Z. Lei, C. Yu, J. Qiu, Adv. Funct. Mater., 2015, **25**,5420-5427.
38 Y. Liu, L. Pan, T. Chen, X. Xu, T. Lu, Z. Sun, D.H.C. Chua, Electrochim. Acta, 2015, **151**, 489-496.
39 D. V. Lam, K. Jo, C. H. Kim, J. H. Kim, H. J. Lee, S. M. Lee, ACS Nano 2016, **10**, 11351-11359.
40 L. Xie, H. Wang, C. Chen, S. Mao, Y. Chen, H. Li and Y. Wang, Research, 2018, **2018**, 5807980.
41 N. Brun, S. R. S. Prabaharan, C. Surcin, M. Morcrette, H. Deleuze, M. Birot, O. Babot, M. F. Achard, R. Backov, J. Phys. Chem. C, 2012, **116**, 1408-1421.
42 B. G. Choi, S. J. Chang, Y. B. Lee, J. S. Bae, H. J. Kim, Y. S. Huh, Nanoscale, 2012, **4**, 5924-5930.
43 Y.M. He, W.J. Chen, X. D. Li, Z.X. Zhang, J.C. Fu, C.H. Zhao, E.Q. Xie, ACS Nano, 2013, **7**, 174–182.
44 T. Kim, J. Yoon, RSC Adv. 2015, **5**, 1456-1461.
45 M.E. Suss, S. Porada, X. Sun, P.M. Biesheuvel, J. Yoon, V. Presser, Energ. Environ. Sci. 2015, **8**, 2296-2319.
46 H.Y. Duan, T.T. Yan, G.R. Chen, J.P. Zhang, L.Y. Shi, D.S. Zhang, Chem. Comm. 2017, **53**, 7465-7468.
47 J. Shen, Y. Li, C. Wang, R. Luo, J. Li, X. Sun, J. Shen, W. Han, L. Wang, Electrochim. Acta, 2018, **273**, 34-42.
48 G. Zhu, H. Wang, H. Xu, L. Zhang, J. Electroanal. Chem. 2018, **822**, 81-88.
49 Y. Li, Y. Liu, M. Wang, X. Xu, T. Lu, C.Q. Sun, L. Pan, Carbon, 2018, **130**, 377-383.
50 J. Li, B. Ji, R. Jiang, P. Zhang, N. Chen, G. Zhang, L. Qu, Carbon 2018, **129**, 95-103.
51 Y. Li, J. Shen, J. Li, X. Sun, J. Shen, W. Han, L. Wang, Carbon, 2017, **116**, 21-32.
52 Z. Chen, H. Zhang, C. Wu, L. Luo, C. Wang, S. Huang, H. Xu, Desalination, 2018, **433**, 68-74.
53 B. Krüner, P. Srimuk, S. Fleischmann, M. Zeiger, A. Schreiber, M. Aslan, A. Quade, V. Presser, Carbon, 2017, **117**, 46-54.
54 L. Zhang, Y. Liu, T. Lu, L. Pan, J. Electroanal. Chem., 2017, **804**, 179-184.
55 Y. Zhang, L. Chen, S. Mao, Z. Zhuo, Y. Song, R. Zhao, J. Colloid. Interf. Sci., 2019, **536**, 252-260.
56 Z. Wang, X. Xu, J. Kim, V. Malgras, R. Mo, C. Li, Y. Lin, H. Tan, J. Tang, L. Pan, Y. Bando, T. Yang, Y. Yamauchi, Materials Horizons, 2019, **6**, 1433-1437.
57 H. Wang, T. T. Yan, L. Y. Shi, G. R. Chen, J. P. Zhang, D. S. Zhang, ACS Sustain. Chem. Eng., 2017, **5**, 3329-3338.
58 C. Wang, H. Song, Q. Zhang, B. Wang, A. Li, Desalination, 2015, **365**, 407-415.
59 T. Wu, G. Wang, S. Wang, F. Zhan, Y. Fu, H. Qiao, J. Qiu, Environ. Sci. Tech. Let., 2018, **5**, 98-102.
60 J. L. Han, T. T. Yan, J. J. Shen, L. Y. Shi, J. P. Zhang, D. S. Zhang, Environ. Sci. Technol.2019, DOI: 10.1021/acs.est.9b04274